International Journal of Concrete Structures and Materials

RESEARCH Open Access

Study on Roof Deterioration Characteristics of Immersed Tunnel Exposed to Fire by Multi-Phase Meso-Model

Wei Wang*, Xuendan Yao, Guiqiang Gao and Yanfei Zhang

Abstract

Deterioration characteristics analysis of lining structure has received intense research interests for immersed tube tunnel fire, while a considerable part of the spotlight is on numerical simulation. However, most of existing works consider concrete lining as a macroscopic homogeneous material for simulation analysis, ignoring the difference of its internal components. This paper aims at studying the mesoscopic deterioration characteristics of immersed tube tunnel roof structure towards efficient safety design of immersed tube tunnel roof. In particular, we establish a mesoscopic model of immersed tube tunnel under thermo-mechanical coupling using ANSYS. Compared with the traditional homogeneous approaches, the proposed mesoscopic model can directly simulate the fire degradation process of immersed tube tunnel roof structure, which blazes marvelous trail for related engineering applications. Our extensive simulation results reveal the progressive failure process of micro-cracks initiation, development, expansion and coalescence in the roof of immersed tube tunnel.

Keywords: immersed tube tunnel, reinforced concrete structure, mesoscopic damage, fire, degradation characteristics

1 Introduction

In order to break the regional division and strengthen the regional connection, China has established a large trans-river and sea channel in the coastal areas as the connecting instrument of multi-regional economy, which greatly improves the resilience of the coastal areas' economy. Among the large trans-river–sea passages that can be used commercially at present, immersed tube tunnel has the advantages of strong formation adaptability, short construction period and strong ability to resist natural disasters at sea, which has gradually become the preferred scheme for large trans-river–sea passages in the future (Kurbatcky & Pestriakova, 2019; Lai et al., 2017; Ren et al., 2019; Sýkora et al., 2018). But during the operation of the tunnel, fire, as a major disaster, also occurred frequently. Since the immersed tube tunnel is a long and narrow structure located in an underground or underwater environment (Zhu et al., 2019), once a fire occurs, there will often be significant casualties and huge economic losses, and the bearing capacity and service life of the tunnel will be affected as well. Therefore, it is inevitable to consider the impact of fire in the immersed tube tunnel, and fire prevention is an important issue that must be faced in the construction and operation of cross-river–sea tunnels all over the world.

The fire safety of immersed tunnels is being increasingly studied worldwide (Vuilleumier et al., 2002; Xu et al., 2018). Broadly speaking, methods in the literature of immersed tube tunnel fire can be divided into experiment, numerical simulation and combination of experiment and numerical simulation. Experimental method can observe the results intuitively, while the numerical simulation can save a lot of cost and time, and realize the

*Correspondence: wangweicsu@csu.edu.cn
School of Civil Engineering, Central South University, Changsha 410075, China
Journal information: ISSN 1976-0485 / eISSN 2234-1315

setting of complex working conditions. At present, there are 1:1 full-scale model (Xu et al., 2018) and 1:5 scale model (Duan et al., 2021; Lin et al., 2021) for immersed tube tunnel of Hong Kong–Zhuhai–Macau Bridge in the literatures. The temperature field distribution (Jiang et al., 2018; Xi et al., 2020), structural damage analysis (Guo et al., 2016), smoke flow law (Lee et al., 2010; Liu et al., 2021; Xu et al., 2019), mechanical ventilation performance (Li et al., 2021), personnel evacuation (Tian & Jiang, 2018) and fire resistance of immersed tube tunnel (Choi et al., 2011) have been studied extensively.

Moreover, fire spalling of tunnel concrete is more a material-level behavior than a structural-level behavior. The moisture inside the concrete will migrate when it is exposed to fire. At the same time, the compressive strength, elastic model, thermal expansion rate and other changes of concrete have an impact on the fire resistance of the overall structure (Akca & Özyurt, 2018; Chen et al., 2020; Kamen et al., 2008; Ryu et al., 2018). Nevertheless, existing researches mainly describe and statistics the macroscopic phenomena of tunnel structure under fire, although the research focus has gradually shifted to mesoscopic component of concrete that can reflect the overall mechanical properties of concrete structures (Jin et al., 2020; Wang et al., 2018a; Wang et al., 2018b; Zhao et al., 2011). Meanwhile, few scholars have discussed the mesoscopic deterioration characteristics of immersed tube tunnels under fire.

The paper established a mesoscopic model of immersed tube tunnel roof, which takes immersed tunnel roof as the research object and considers the decisive influence of meso-structure on macroscopic mechanical behavior. Through the establishment of this model, the mesoscopic damage law of fire sinking tube tunnel roof can be clarified, and the gradual damage process of micro-cracks initiation, development, expansion and connection in fire sinking tube tunnel roof can be revealed.

2 Material Parameters and Methods

2.1 Thermodynamic Parameters of Reinforced Concrete at High Temperature

Different from the general macro-model, the analysis of reinforced concrete model under fire needs to consider the high-temperature mechanical properties of materials, in which the thermodynamic parameters mainly include specific heat capacity, thermal conductivity, convective heat transfer coefficient and thermal expansion coefficient.

In this paper, thermal conductivity and specific heat capacity of concrete at high temperature recommended by European standards are adopted. Thermal expansion coefficient is obtained by transforming the coefficient of thermal expansion studied by Yan, 2015 and Xiao et al., 2018. In addition, only convective heat transfer is considered. Convective heat transfer coefficient is calculated using the empirical formula proposed by Duan, 1985. Specific figures are shown in Table 1. Meanwhile, thermal conductivity, specific heat capacity and linear expansion coefficient of steel bars are shown are shown in Table 1.

For the thermal parameters of mesoscopic materials, thermal expansion coefficient, thermal conductivity and specific heat capacity of aggregate and mortar are shown in Formulas (1–4). Thermal parameters of interface layer are consistent with mortar:

$$k_T = 1.36 - 0.136\left(\frac{T}{100}\right) + 0.0057\left(\frac{T}{100}\right)^2, \quad (1)$$

$$k_{aT} = \frac{770}{0.84(350+T)} + 0.7, \quad (2)$$

$$C_T = 790 + 0.9T \quad (3)$$

$$C_{aT} = 625 \times (1+T)^{0.075}. \quad (4)$$

2.2 High-Temperature Damage Constitutive Model

High-temperature damage constitutive relationships of concrete, its meso-phase materials, and steel bars are shown in Table 2.

2.3 Random Aggregate Delivery Method

In engineering application, the aggregate inside concrete is scattered and irregular in spatial distribution, and the quantity is usually large. For this reason, Monte Carlo method can be used to solve the randomness problem in modeling. In this paper, APDL language in ANSYS is used to establish the coordinates and diameters of randomly distributed aggregate, and a large number of RANDOM Numbers are generated between (0,1) by RANDOM command, and then multiplied with the spatial coordinates and radii of aggregate to obtain the coordinates and diameters of randomly distributed aggregate. In order to make the aggregate independent, non-overlapping and within a certain area of placement, the following three criteria are established, where, whether the aggregate exceeds the feeding area can be determined by Formula (5):

$$\begin{pmatrix} x \\ y \end{pmatrix} = \begin{pmatrix} x_i \\ y_i \end{pmatrix} + \begin{pmatrix} r_i \\ r_i \end{pmatrix} + \begin{pmatrix} d_i \\ d_i \end{pmatrix} \in \begin{bmatrix} (x_{\min}, x_{\max}) \\ (y_{\min}, y_{\max}) \end{bmatrix}, \quad (5)$$

where x_i, y_i, r_i are, respectively, the horizontal and vertical coordinates of a circle and the radius values of a circle of a random aggregate; d_i is the thickness of boundary layer;

Table 1 Thermodynamic parameter curve of reinforced concrete at high temperature.

Materials	Concrete	Steel bars
Thermal conductivity	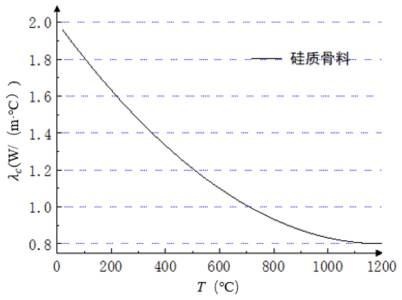	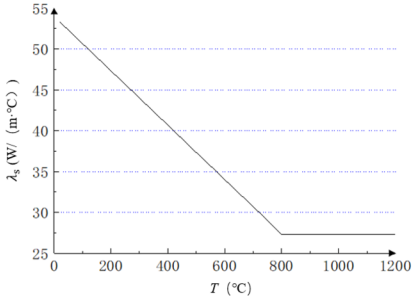
Specific heat capacity	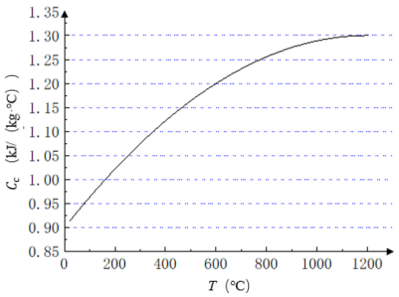	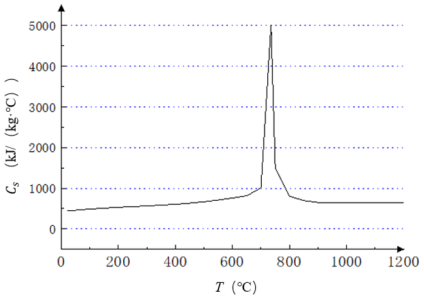
Thermal expansion coefficient	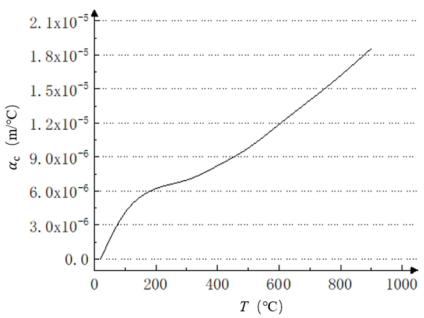	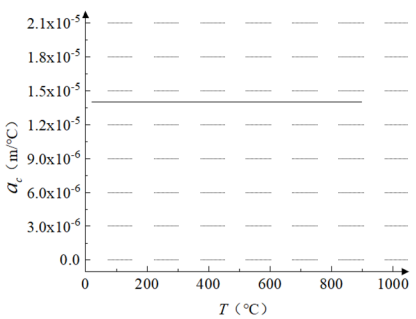
Convective heat transfer coefficient	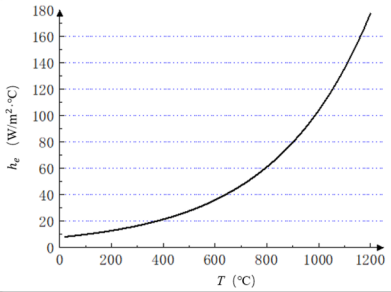	/

$x_{\min}$, $x_{\max}$ is the minimum and maximum of the horizontal coordinate values of the analysis area of the mesoscopic model; $y_{\min}$, $y_{\max}$ is the minimum and maximum value of vertical coordinate values in the analysis area of the mesoscopic model.

The aggregate coincides can be determined by Formula (6):

$$\sqrt{(x_i - x_j)^2 + (y_i - y_j)^2} > r_i + r_j + 2d. \tag{6}$$

The aggregate overlaps with the reinforcement can be determined by Formula (7) (assuming that the reinforcement is parallel to the X-axis):

Table 2 High-temperature constitutive relation of reinforced concrete components.

Materials	High temperature damage constitutive mode	Materials	High temperature damage constitutive mode
Concrete	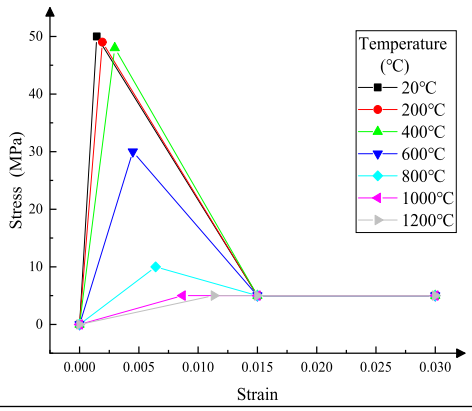	Aggregate	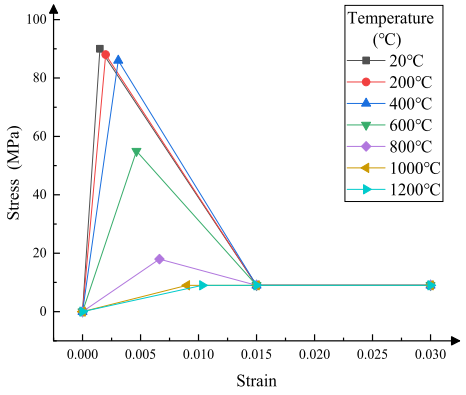
Mortar	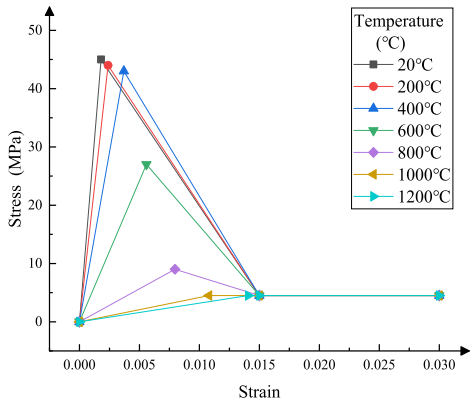	Interlayer	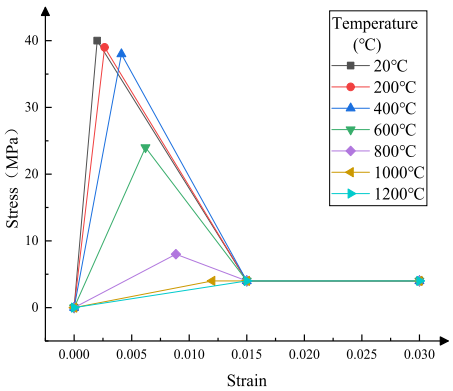
Steel bars	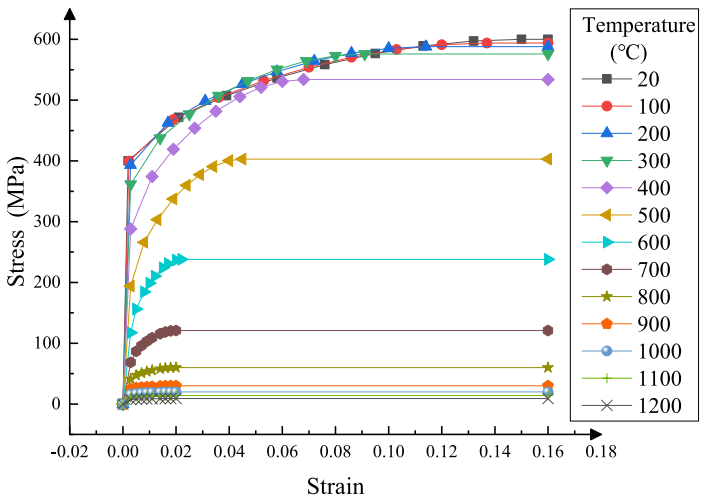		

$$|y_i - b| > r_i, \tag{7}$$

where y_i, r_i is the circular ordinate and radius of a random aggregate and b is the distance between the reinforcement and the X-axis.

There will be a certain gap between the aggregates in the concrete. At the same time, there is also a weak contact transition section between the aggregate and the mortar—the interlayer. In the random aggregate model, a separate analysis area must be established for the

boundary layer. In the algorithm in this paper, the initial radius of aggregate delivery is the sum of the theoretical radius and the thickness of the interface layer. Finally, the concentric circle is used to generate the aggregate consistent with the theoretical radius, so as to establish the interface layer of 1 mm.

Walraven J. C established the relationship between concrete gradation curve and aggregate interface area in a single section [Formula (8)], which can be applied in microscopic analysis for two-dimensional plane analysis:

$$\begin{aligned} P_c(D < D_0) = P_k(&1.065D_0^{0.5}/D_{\max}^{0.5} \\ &-0.053D_0^4/D_{\max}^4 - 0.012D_0^6/D_{\max}^6 \\ &-0.0045D_0^8/D_{\max}^8 + 0.0025D_0^{10}/D_{\max}^{10}), \end{aligned} \tag{8}$$

where P_k is the percentage of aggregate volume in the total volume of concrete; D_0 is the diameter of sieve hole; and $D_{\max}$ is the maximum aggregate particle size.

The concrete mesoscopic model established in this paper simplifies the aggregate to circular, which is different from the polyhedral aggregate in engineering practice. However, scholars (Ji, 2014; Li, 2012, 2016) have obtained good results in the meso-analysis of the mechanical properties of concrete structures. We found that the analysis results using spherical and irregular polygons are similar, so it is in line with the actual situation to simplify the aggregate into a circular to a certain extent.

3 Establishment of Local Mesoscopic Model of Immersed Tube Tunnel

Geometric dimensions of the structure are mainly referred to the construction drawing design of Hong Kong–Zhuhai–Macao Bridge. The cross-sectional dimensions and specific reinforcement are shown in Fig. 1. In this paper, the form of reinforcement is simplified. Only the influence of main reinforcement is considered. Lines marked by blue represent HRB400 steel bars with a diameter of 40 mm, while those marked by red at the flue represent HRB400 steel bars with a diameter of 28 mm. Others are HRB400 steel bars with a diameter of 32 mm. In addition, only half of the model is selected for structural calculation in order to simplify the calculation, and symmetrical boundary conditions are designed in the center of the whole structure.

3.1 Set Fire Scenarios

According to the requirements of 'Code for Fire Protection of Building Design' GB 50016-2014 (2018 edition), Hong Kong–Zhuhai–Macao immersed tunnel belongs to I class of tunnels, whose fire resistance limit should not be less than 2 h and fire resistance limit test curve should adopt the RABT standard heating curve. Therefore, RABT standard heating curve will be used as immersed tunnel fire scenarios in this paper. The specific expression is shown in Formula (9):

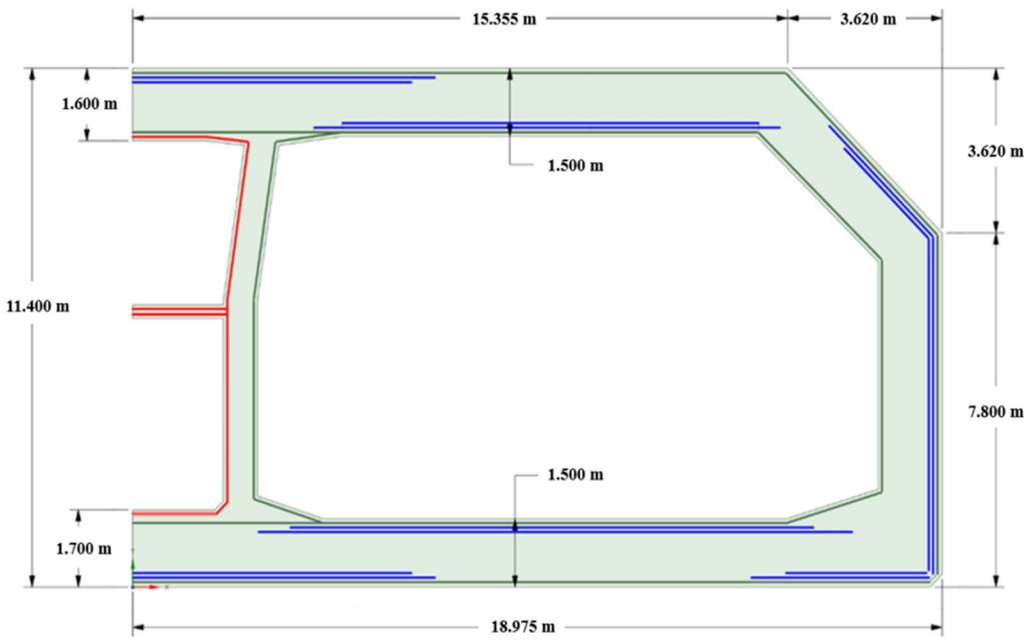

Fig. 1 Schematic diagram of immersed tube tunnel structure.

$$T = \begin{cases} T_0 + 236 \times t & t \le 5 \text{ min} \\ T_0 + 1180 & 5 \text{ min} \le t \le 95 \text{ min} \\ 1200 - 40.333 \times (t - 95) & 95 \text{ min} \le t \le 125 \text{ min} \end{cases}, \quad (9)$$

where t is time and T_0 is the initial temperature.

3.2 Boundary Condition

Due to the short fire time, temperature of concrete on the unburned side (i. e., the junction of water and soil around immersed tunnel and immersed tunnel) will not be affected. Therefore, we ignore the heat exchange between the surrounding water and soil environment and the immersed tunnel in the calculation, and assume the boundary temperature of the concrete without fire is 20 ℃. It is assumed that the main loads borne by immersed tunnel are vertical water and soil pressure, horizontal water and soil pressure, vehicle load and self-weight. Referring to the stratum conditions of Hong Kong–Zhuhai–Macao immersed tunnel and related literature (Jiang & Chen, 2015; Zhang, 2013), the load diagram of the cross section can be calculated by using the load-structure method. Fire seat is determined to be 1.8 m high from the bottom plate in the middle of the tunnel. Temperature and load arrangement are shown in Fig. 2.

3.3 Determination of the Most Unfavorable Position of Immersed Tunnel Roof

Obviously, it is time-consuming and laborious to establish a mesoscopic model of full-scale immersed tunnel. Moreover, the failure process of tunnel roof is often restricted by local failure, which can also reflect the overall failure to some extent. Therefore, the most unfavorable position of immersed tunnel roof under thermal coupling will be explored below. Fig. 3 is the vertical displacement diagram of each monitoring point at different times of immersed tunnel roof.

It can be seen from Fig. 3 that the vertical displacement trend of the roof under the action of no fire and different fire time is consistent, which shows that fire does not cause too much influence on the overall trend of the vertical deformation of the whole tunnel roof. Although the position of the maximum displacement of the immersed tube tunnel roof will change at different times, it is roughly between monitoring point 3 and monitoring point 4. Side wall at the exhaust duct causes a large reverse bending moment on the left side of the roof, which causes the peak point of vertical displacement at the bottom of the roof to deviate from the center line of the roof. The position of the maximum settlement of the immersed tunnel roof is 10.3 m away from the structural center line (measuring point 3 is 9.775 m away from the structural center line), and the maximum settlement is 5.1 mm without fire. Within 125 min of fire, the maximum settlement is 5.6 mm, which can reflect the actual deformation characteristics of immersed tunnel to a certain extent (Jiang & Chen, 2015; Zhang, 2013).

3.4 Establishment of Local Mesoscopic Model of Immersed Tunnel Roof

This article only conducts random aggregate delivery in the dangerous area of the roof (10.3 m from the centerline of the tunnel) to establish a local Mesoscopic model. In view of the weak position of the submerged tunnel

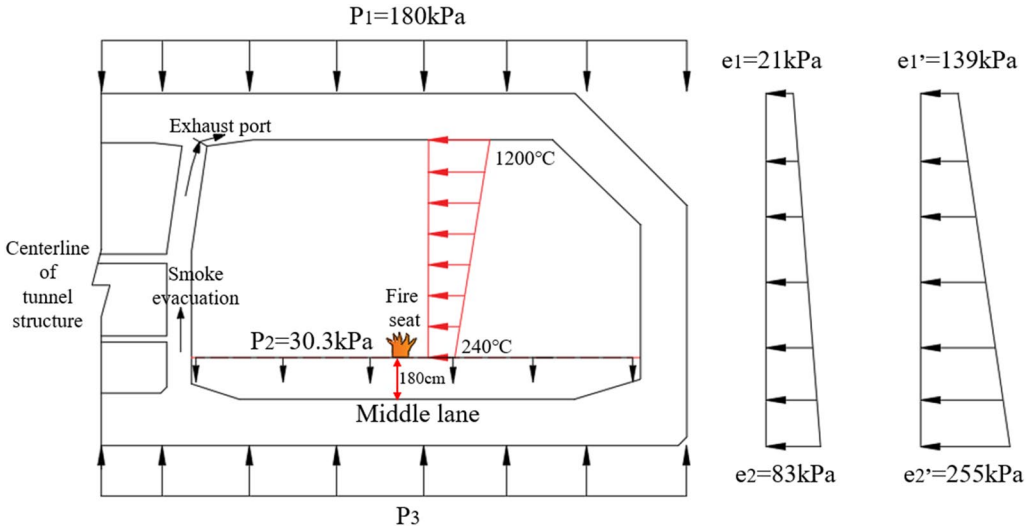

Fig. 2 Fire scenarios and load distribution of immersed tube tunnel.

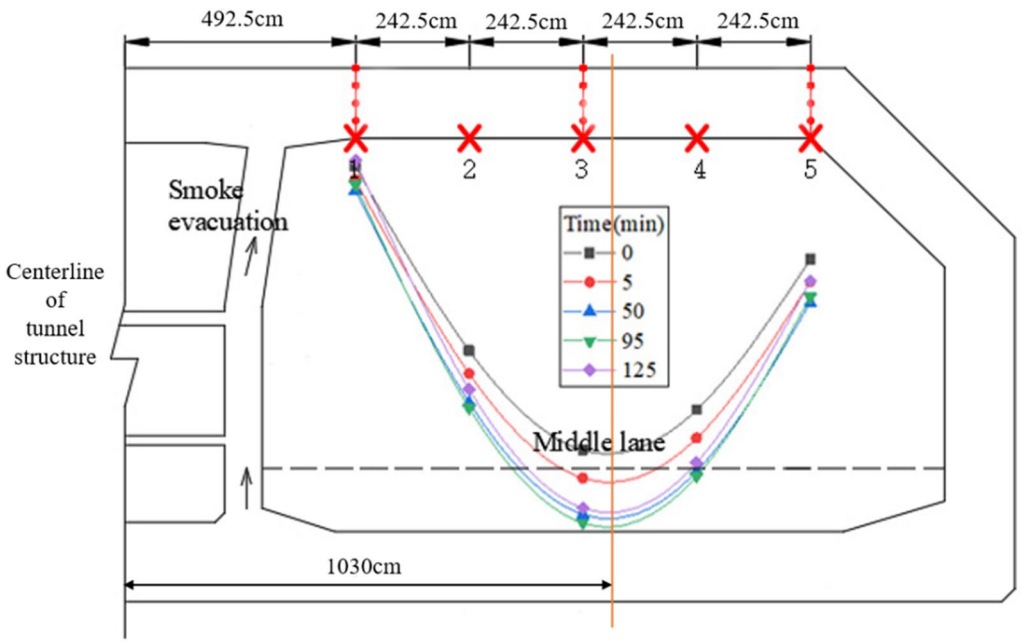

Fig. 3 Vertical displacement diagram of each monitoring point at different times.

roof, local meso-models are established in the middle of the roof fire zone and the upper compression zone, whose area is 300×300 mm. In addition, the roof of immersed tube tunnel is made of C50 concrete of two-grading. According to the existing grading regulations, the particle size ranges of 5–20 mm and 20–40 mm are selected, while the aggregate below 5 mm is included in the mortar. Seventy percent aggregate filling rate is adopted. By calculation, 192 aggregates with random size particle sizes in the range of 5–20 mm and 23 aggregates with random size particle sizes in the range of 20–40 mm can be obtained. Total number of aggregates is 215.

The model was established by ANSYS (ANSYS WORKBENCH 19.2). Homogeneous concrete, aggregate, mortar and interlayer adopt Plane188 element, while steel rebars adopt Link180 element. Foundation springs adopt Combine39 element which is set on the sides and bottom of the tunnel. In ANSYS, there is no spring element that is only subjected to compression. The author customizes its elastic resistance coefficient based on the characteristics of Combine39 element. We set the elastic resistance coefficient of the spring element to 1 N/m. When it is tensioned, the elastic resistance coefficient is consistent with the actual formation resistance coefficient, so as to approximate the simulation of only compression spring element. The horizontal trapezoidal load and the vertical load are superimposed on the boundary line of the two-dimensional plane element using Surf156 elements.

In addition, in order to facilitate classification and analysis, the meso-models on the top and lower sides are marked as U and N, respectively, as shown in Fig. 4.

This paper mainly considers the variation characteristics of the main strain in the mesoscopic model. In order to facilitate the subsequent analysis, meso-model N is divided into three parts, I, II and III. Each part is 10 cm thick, as shown in Fig. 5.

4 Results and Analysis

4.1 Temperature Field Distribution of Meso-Model N

In order to more clearly characterize the temperature field distribution of concrete at the bottom of the roof, the vertical measurement line is established along the thickness direction in the center of the meso-model N. It can be seen from Fig. 6 that temperature within 15 cm of the roof is below 100 °C when the RABT heating curve continues for 125 min. From Fig. 6, we can see that the heating rate of the concrete far from the fire side is lower when the temperature of the fire curve increases, and similarly, the temperature decreasing rate is also lower when the temperature is lowered. This clearly reflects the thermal inertia of concrete.

Combined with Fig. 7, we found that the surface concrete temperature of about 2 cm reaches 800 °C, whose strength is completely lost. Furthermore, the concrete temperature of 2–6.6 cm is between 380 and 800 °C, and its strength is basically lost.

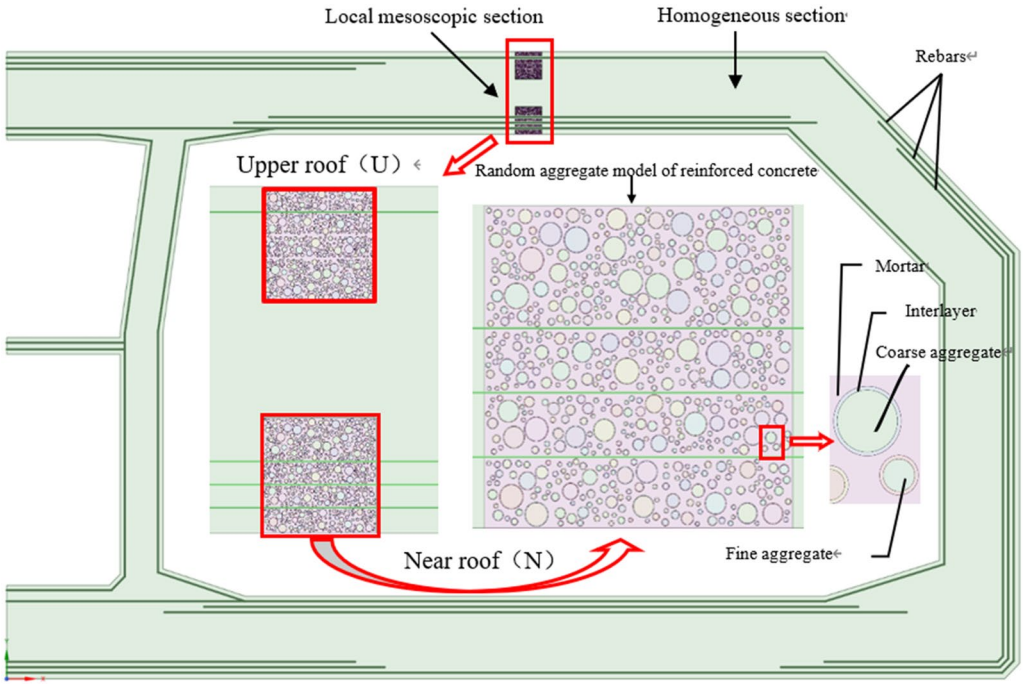

Fig. 4 Local mesoscopic model of reinforced concrete.

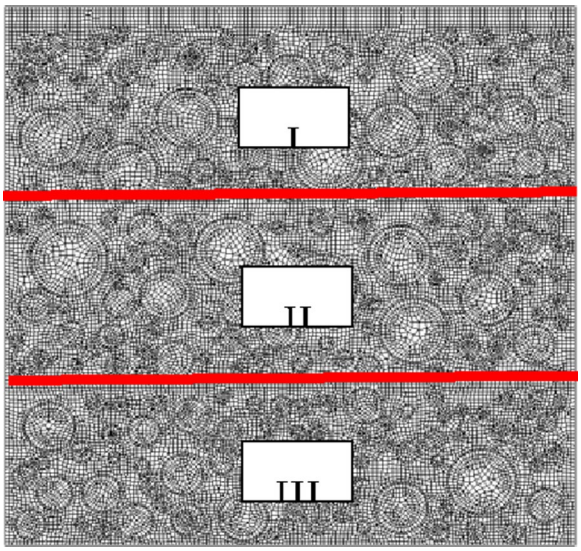

Fig. 5 Meso-model N partition diagram.

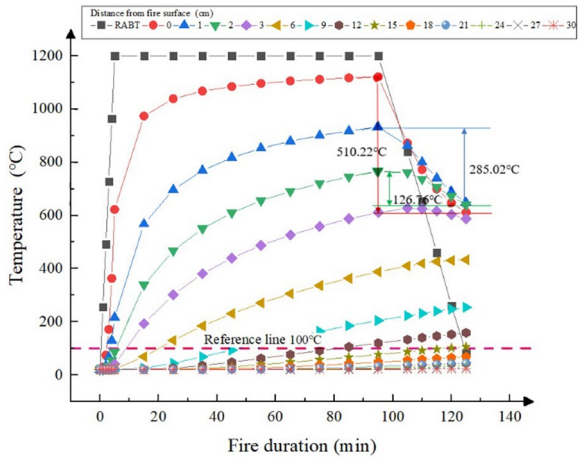

Fig. 6 Internal temperature of model N varies with the fire time.

4.2 Distribution of Maximum Principal Strain of Meso-Model N

Fig. 8 shows the maximum principal strain distribution of meso-model N under different fire time.

After 5 min of fire, the temperature increased rapidly. Large tensile strain also occurs in the lower temperature region, but the damage mainly occurs in the region III. At about 35 min, the damage was further expanded, and a large strain was generated on both sides of the aggregate, indicating that there was a large stress concentration

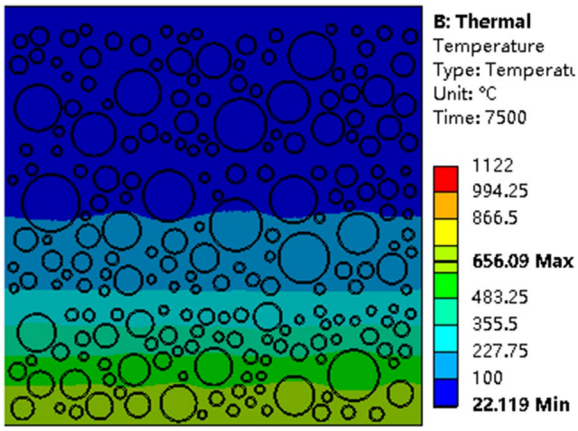

Fig. 7 Temperature field distribution diagram of the roof meso-model N when exposed to fire for 125 min.

between the two sides of the aggregate and the mortar. Large tensile strain can be observed around the aggregate in region I after 65 min of fire. When the duration of fire reaches 95 min, the constant temperature section of RABT heating curve ends, and the temperature in region I is basically equal to or close to normal temperature (20 °C). There will be no strain increase due to material deterioration caused by high temperature. Thus, this region is mainly caused by tensile damage caused by positive bending moment and thermal expansion of concrete near the bottom. On the contrary, the temperature of concrete in zone II is about 50–150 °C, which produces a certain additional compressive stress under the leading role of thermal expansion, so it remains in a relatively safe stress state. After cooling for 15 min, the concrete temperature at the bottom of the roof began to decrease and the strain began to recover.

4.3 Distribution of Minimum Principal Strain Of Meso-Model N

Fig. 9 is the minimum principal strain distribution of the meso-model N under different fire time. It can be seen from the figure that under the influence of thermal expansion, region III has been in a state of large compressive stress, and its damage development is basically consistent with that formed by the maximum principal

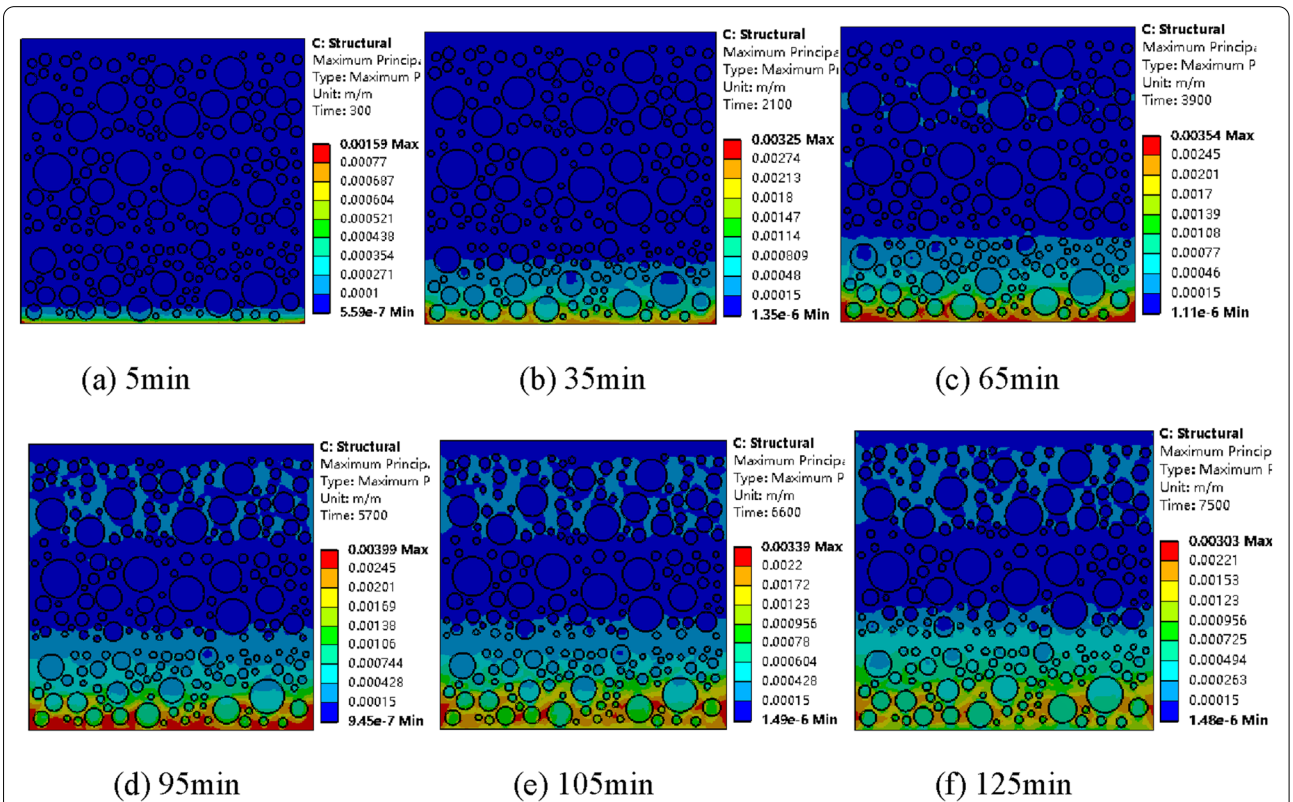

Fig. 8 Distribution of the maximum principal strain of the meso-model under fire for 5/35/65/95/105/125 min: **a** 5 min, **b** 35 min, **c** 65 min, **d** 95 min, **e** 105 min, **f** 125 min.

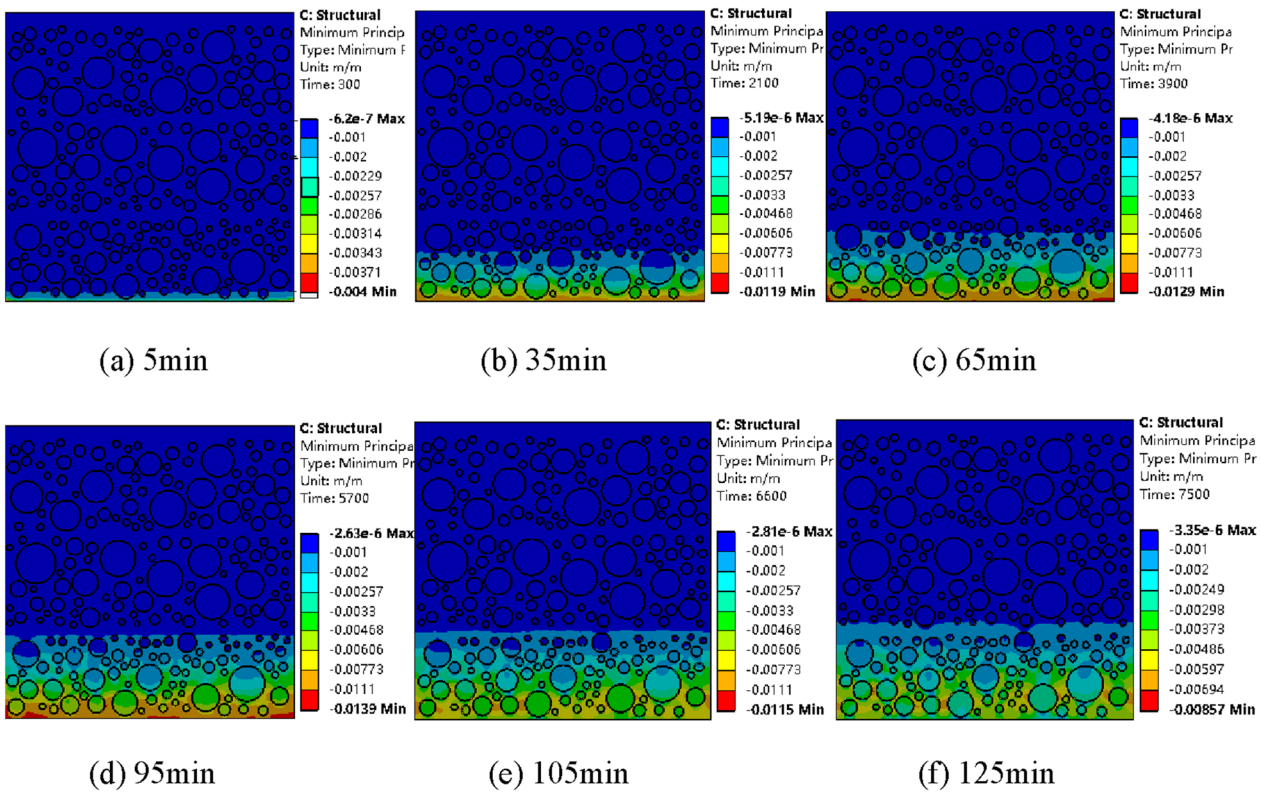

Fig. 9 Distribution of the minimum principal strain of the meso-model under fire 5/35/65/95/105/125 min: **a** 5 min, **b** 35 min, **c** 65 min, **d** 95 min, **e** 105 min, **f** 125 min.

strain distribution. Notably, there was no damage in the roof after 125 min of fire, indicating that the damage in regions II and I is mainly controlled by tensile stress.

4.4 Analysis of Strain Characteristics of Roof Meso-Model U

Fig. 10 is the minimum strain distribution diagram of the meso-model U. It can be seen from the diagram that the compressive strain inside the roof decreases continuously within 125 min of fire, and the maximum compressive strain also decreases from 0.000246 to 0.000095. This is because in the process of fire, the concrete in the bottom of the roof under the thermal expansion area undertakes most of the pressure load, so that the compressive stress of the concrete in the non-fire area has been reduced. Although the compressive strain in meso-model U is less than the strain corresponding to the peak stress during the whole fire process, there is a large concentrated strain around the aggregate. It also can be seen from the cloud image that the strain between aggregate and aggregate has a trend of connection in mortar, indicating that the degradation characteristics of meso-model U are basically consistent with that of meso-model N at room temperature.

4.5 Progressive Failure Process of Meso-Model N

In order to clarify the internal deterioration of immersed tunnel roof, referring to previous research results (Li, 2016; Wang et al., 2018a; Wang et al., 2018b), it is defined that the tensile strain of each meso-material unit of concrete is greater than 0.00015, the compressive strain is greater than 0.002, and the failure occurs when the temperature is higher than 380 °C. Therefore, the progressive failure diagram of the meso-model degradation of the roof of the fire sinking tunnel is obtained (Fig. 11), in which the white part represents the failure area.

After 5 min of fire, due to the rapid increase of temperature, the surface layer of the fire surface of the roof has been damaged in a large area. Combined with the analysis results of the internal temperature field of the micro-model, it is found that the main failure area is basically uniform development with 150 °C isothermal line.

After 65 min of fire, the internal micro-cracks in area I develop along the periphery of aggregate, and some

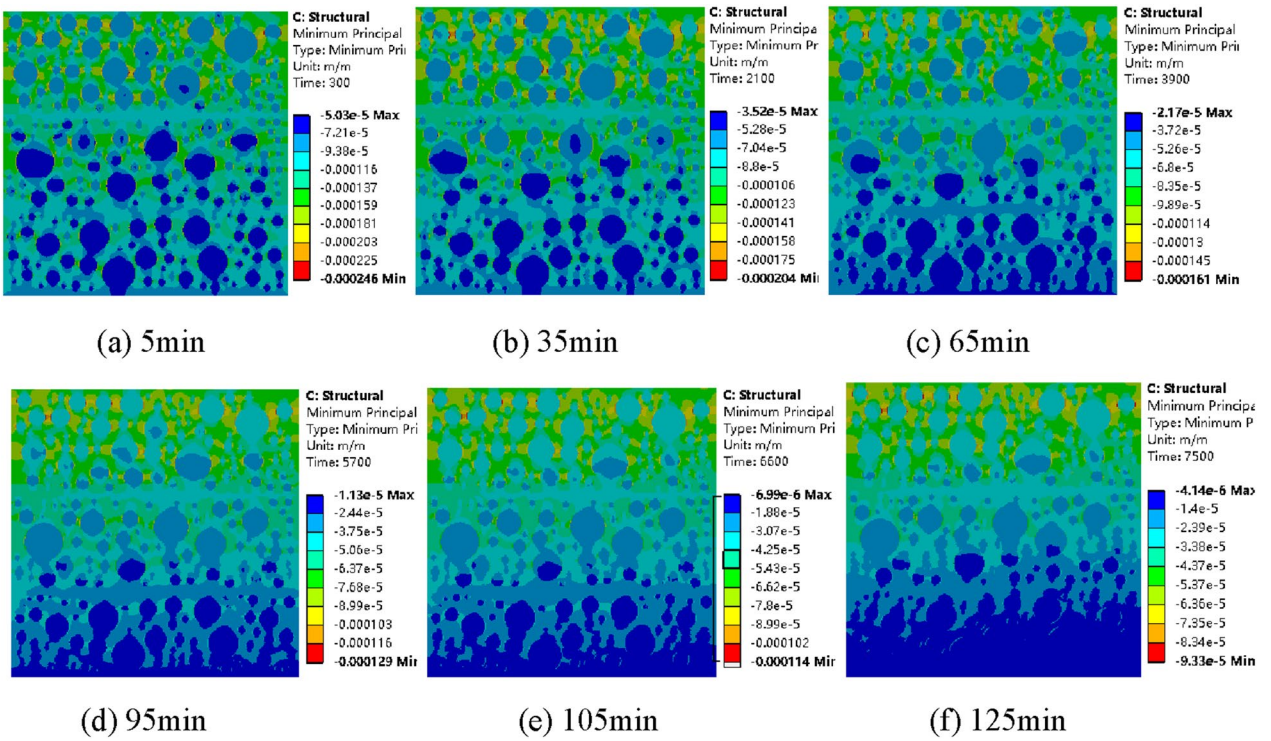

Fig. 10 Distribution of minimum principal strain of meso-model U when exposed to fire for 5/35/65/95/105/125 min: **a** 5 min, **b** 35 min, **c** 65 min, **d** 95 min, **e** 105 min, **f** 125 min.

micro-cracks have penetrated into the mortar area in the process of further degradation, forming large cracks. But unlike region III, aggregate in region I was not damaged.

After 95 min of fire, longitudinal penetrating cracks along the thickness direction of roof have been formed in region I, while the failure development of region III has gradually slowed down. From 95 to 125 min, the temperature of the external environment has gradually decreased to normal temperature, but the damage range of region I and region III is still expanding, and more cracks begin to erupt in region II. The maximum stress damage depth obtained in this paper is about 28 cm, and the maximum damage depth calculated by Guo et al. (2016) is 25 cm, which can prove the reliability of the simulation. At the same time, the research results (Li et al., 2011; Ma et al., 2004) on meso-damage of concrete are similar to those obtained by this simulation.

Fig. 12 shows the variation curve of damage ratio of each meso-material with fire time. The progressive deterioration process of concrete at meso-level can also be seen from the diagram.

5 Conclusions

In the present study, a local mesoscopic model is established for the dangerous area of immersed tube tunnel roof. Numerical simulation results are present in this paper. Based on the phenomena and data of the simulation, following conclusions can be drawn:

(1) In the mesoscopic model, the section loss caused by high temperature is about 6.6 cm, while the maximum stress damage along the thickness direction is about 28 cm, which is basically consistent with the relevant research results. Compared with mortar and boundary layer, aggregate damage has a certain hysteresis. In the normal temperature area, aggregates will not be damaged even if the crack penetrates.

(2) Deterioration of concrete is a gradual process in meso-scale. In the high-temperature area on the fire side of the roof, the interlayer with lower strength is destroyed first and produces micro-cracks. However, the meso-damage of concrete in this area

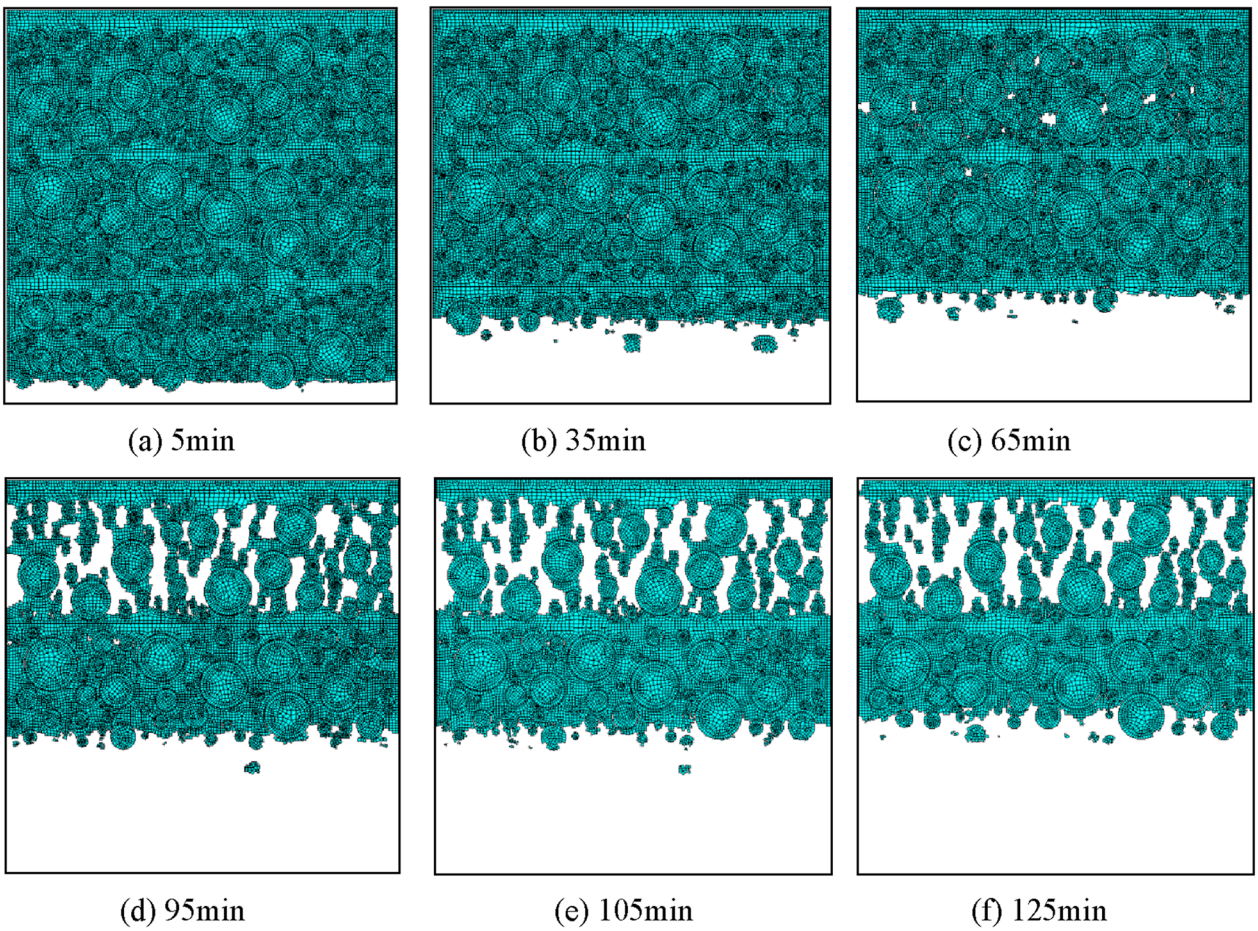

Fig. 11 Progressive destruction of the meso-model model when exposed to fire for 5/35/65/95/105/125 min: **a** 5 min, **b** 35 min, **c** 65 min, **d** 95 min, **e** 105 min, **f** 125 min.

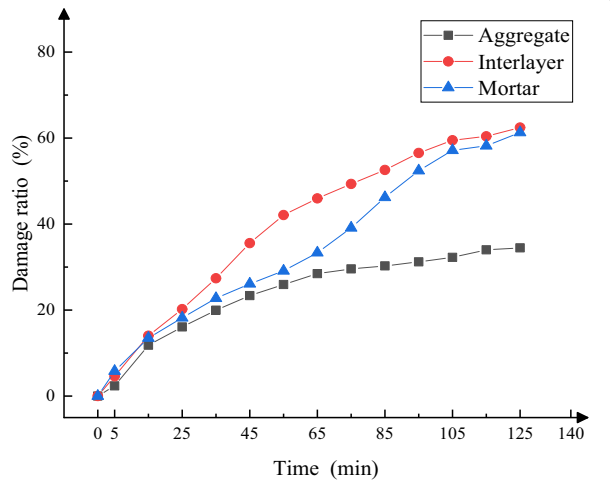

Fig. 12 The change curve of meso-material damage ratio with time.

uniformly develops inward due to the rapid transmission of high-temperature damage. In the normal temperature area inside the roof, the concrete will produce large tensile stress driven by thermal expansion, and the micro-cracks around the aggregates will further deteriorate, forming longitudinal through cracks in the mortar.

Acknowledgements
The authors would like to thank the members of the SJL 1012-2 office for their selfless help and useful suggestions.

Authors' contributions
All authors contribute equally to this paper. WW and XY wrote the first draft of the paper. XY, GG and YZ are responsible for model conduction, analysis and interpretation. All authors read and approved the final manuscript.

Author information
Wei Wang, Associate Professor, School of Civil Engineering, Central South University, Changsha, 410075, China. Xuedan Yao, Master Student, School of

Civil Engineering, Central South University, Changsha, 410075, China. Guiqiang Gao, Master Student, School of Civil Engineering, Central South University, Changsha, 410075, China. Yanfei Zhang, Master Student, School of Civil Engineering, Central South University, Changsha, 410075, China.

Funding
This work was supported by the Natural Science Foundation of Hunan Province (No. 2018JJ2519).

Availability of data and materials
The data and materials had been included in the manuscript.

Declarations

Competing interests
The authors declare no competing interests.

Received: 4 September 2021 Accepted: 28 January 2022
Published online: 08 March 2022

References

Akca, A. H., & Özyurt, N. (2018). Deterioration and recovery of FRC after high temperature exposure. *Cement and Concrete Composites, 93*, 260–273.
Chen, X. D., Shi, D. D., & Guo, S. S. (2020). Experimental study on damage evaluation, pore structure and impact tensile behavior of 10-year-old concrete cores after exposure to high temperatures. *International Journal of Concrete Structures and Materials, 14*(1), 1–17.
Choi, S. W., Chang, S. H., Kim, H. Y., & KJo, B. H. (2011). Experimental evaluation of fire protection measures for the segment joint of an immersed tunnel. *Journal of Korean Tunnelling and Underground Space Association, 13*(3), 177–197.
Duan, J. T., Dong, Y. L., Xiao, J. Z., Zhang, D., Zheng, W., & Zhang, S. (2021). A large-scale fire test of an immersed tunnel under the protection of fire resistive coating. *Tunnelling and Underground Space Technology, 111*, 103844.
Duan, W. X. (1985). Fire analysis and treatment of building structures calculation of fire temperature fields. *Industrial Construction, 1*(8), 51–54.
Guo, J., Jiang, S. P., & Zhang, Z. Y. (2016). Fire thermal stress and its damage to subsea immersed tunnel. *Procedia Engineering, 166*, 296–306.
Ji, S. H. (2014). *Numerical simulation of meso-structure and failure process of fiber reinforced concrete*. Changan University.
Jiang, S. P., & Chen, Y. (2015). *Research on joint and structure fire prevention technology of offshore extra-long immersed tube tunnel*. Chongqing Jiaotong University.
Jiang, S. P., Tian, K., & Xu, P. (2018). Distribution laws of fire temperature fields in immersed tunnel: A case study of Hong Kong–Zhuhai–Macao Bridge immersed tunnel project. *Tunnel Construction, 38*(05), 719–729.
Jin, L., Lan, Y. C., Zhang, R. B., & Du, X. (2020). Impact resistances of RC beams at/after high temperature: Meso-scale analysis. *Scientia Sinica Physica, Mechanica & Astronomica, 50*(2), 024613.
Kamen, A., Denarié, E., Sadouki, H., & Brühwiler, E. (2008). Thermo-mechanical response of UHPFRC at early age—Experimental study and numerical simulation. *Cement and Concrete Research, 38*(6), 822–831.
Kurbatcky, E., & Pestriakova, E. (2019). Advantages of immersed tunnels for long water crossings. *MATEC Web of Conferences, 265*, 5021.
Lai, J. X., Zhou, H., Cheng, F., Wang, H., & Feng, Z. H. (2017). Statistical analysis of fire accidents in highway tunnels and countermeasures for disaster prevention. *Tunnel Construction, 37*(4), 409–415.
Lee, E. J., Oh, C. B., Oh, K. C., Yoo, Y. H., & Shin, H. J. (2010). Performance of the smoke extraction system for fires in the Busan–Geoje immersed tunnel. *Tunnelling and Underground Space Technology, 25*(5), 600–606.
Li, B. D. (2012). *Mesoscopic analysis and numerical simulation of mechanical properties for recycled concrete composite materials with interface*. South China University of Technology.
Li, D. (2016). *High temperature damage of concrete based on meso-mechanics and response of immersed tunnel structure in fire*. Central South University.
Li, C. H., Wang, H. L., & Xu, G. X. (2011). Three-dimensional microscopic numerical simulation of concrete damage fracture. *Journal of Central South University (Natural Science Edition), 42*(2), 463–469.
Li, L. J., Qiu, Q. Z., Zhang, X. F., Xu, P., Liu, J., Li, Y., & Fan, C. (2021). Assessment of different ventilation strategies on ventilation performance in immersed tunnels. *Environmental Science and Pollution Research*.
Lin, J. Q., Dong, Y. L., Duan, J. T., Zhang, D., & Zheng, W. (2021). Experiment on single-tunnel fire in concrete immersed tunnels. *Tunnelling and Underground Space Technology, 116*, 104059.
Liu, S. L., Wang, L., Yu, M. G., & Jiang, Y. D. (2021). Optimization of smoke exhaust efficiency under a lateral central exhaust ventilation mode in an extra-wide immersed tunnel. *Journal of Zhejiang University-Science A, 22*(5), 396–406.
Ma, H. F., Chen, H. Q., & Li, B. K. (2004). Numerical simulation of concrete specimen microstructure. *Chinese Journal of Water Resources, 1*(10), 27–35.
Ren, R., Zhou, H., Hu, Z., He, S., & Wang, X. (2019). Statistical analysis of fire accidents in Chinese highway tunnels 2000–2016. *Tunnelling and Underground Space Technology, 83*, 452–460.
Ryu, E., Shin, Y., & Kim, H. (2018). Effect of loading and beam sizes on the structural behaviors of reinforced concrete beams under and after fire. *International Journal of Concrete Structures and Materials, 12*(1), 1–10.
Sýkora, J., Jarušková, D., Šejnoha, M., & Šejnoha, J. (2018). Fire risk analysis focused on damage of the tunnel lining. *Fire Safety Journal, 95*, 51–65.
Tian, K., & Jiang, S. P. (2018). Reinforcement learning for safe evacuation time of fire in Hong Kong–Zhuhai–Macau immersed tube tunnel. *Systems Science & Control Engineering, 6*(2), 45–56.
Vuilleumier, F., Weatherill, A., & Crausaz, B. (2002). Safety aspects of railway and road tunnel: Example of the Lötschberg railway tunnel and Mont-Blanc road tunnel. *Tunnelling and Underground Space Technology, 17*(2), 153–158.
Wang, H., Binder, E., Mang, H., Yuan, Y., & Pichler, B. (2018). Multiscale structural analysis inspired by exceptional load cases concerning the immersed tunnel of the Hong Kong–Zhuhai–Macao Bridge. *Underground Space, 3*(4), 252–267.
Wang, W., Liu, Ou., Cao, K., & Xu, Z. S. (2018). Meso damage evolution of tunnel lining concrete under fire. *Journal of Zhejiang University (Engineering Science), 52*(5), 906–913.
Xi, Y., Wu, M. J., Cao, P., Chen, J.Z., & Chen, J.T. (2020). Temperature distribution of a composite structure with steel-shell and concrete under high temperature of fire. *Chinese Journal of Underground Space and Engineering, 16*(S2), 985–992.
Xiao, J., Xie, Q., & Xie, W. (2018). Study on high-performance concrete at high temperatures in China (2004–2016)—An updated overview. *Fire Safety Journal, 95*, 11–24.
Xu, P., Jiang, S. P., Xing, R. J., & Tan, J. Q. (2018). Full-scale immersed tunnel fire experimental research on smoke flow patterns. *Tunnelling and Underground Space Technology, 81*, 494–505.
Xu, P., Xing, R. J., Jiang, S. P., & Li, L. J. (2019). Theoretical prediction model and full-scale experimental study of central smoke extraction with a uniform smoke rate in a tunnel fire. *Tunnelling and Underground Space Technology, 86*, 63–74.
Yan, R. Z. (2015). *Influence of high temperature on physical and mechanical properties of C40 high performance concrete*. Taiyuan University of Technology.
Zhang, Z. Y. (2013). *Research of mechanics behavior for immersed tunnel under fire load*. Chongqing Jiaotong University.
Zhao, J., Zheng, J. J., Peng, G. F., & van Breugel, K. (2011). Mesoscopic thermal-mechanical fire damage modeling of high performance concrete. *Advanced Materials Research, 194*, 1095–1098.
Zhu, Y. L., Lin, M., Meng, F. C., Liu, X., & Lin, W. (2019). The Hong Kong–Zhuhai–Macao Bridge. *Engineering, 5*(1), 10–14.

Publisher's Note